Sharp Fe/MgO/Ge(001) epitaxial heterostructures for tunneling junctions

D. Petti,[1,a)] M. Cantoni,[1] C. Rinaldi,[1] S. Brivio,[1] R. Bertacco,[1] J. Gazquez,[2,3] and M. Varela[3]
[1]*L-NESS, Dipartimento di Fisica, Politecnico di Milano, Via Anzani 42, 22100 Como, Italy*
[2]*Department Fisica Aplicada III, Universidad Complutense de Madrid. Avda. Complutense s/n, Madrid 28040, Spain*
[3]*Oak Ridge National Laboratory, Oak Ridge TN 37831, USA*

(Received 14 September 2010; accepted 13 January 2011; published online 22 April 2011)

We report on the growth of epitaxial Fe/MgO/Ge(001) heterostructures by molecular beam epitaxy. The lowest oxidation and highest sharpness of the MgO/Ge interface, corresponding to a transition layer on the order of one Ge unit cell, is obtained for room temperature growth of the MgO layer followed by annealing in a vacuum at 500 °C. In these conditions, the MgO layer grows epitaxially on Ge(001) with the [110] direction parallel to the [100] direction of Ge, at variance with the cube-on-cube growth on Si(001) and GaAs(001). However, in some cases, the cube-on-cube growth mode of MgO on Ge competes with the mode involving a 45° rotation, as revealed by transmission electron microscopy and photoelectron diffraction data on MgO films grown at 300 °C without postannealing, and on p-doped Ge substrates. For the Fe overlayer, in all the cases reported, room temperature growth followed by annealing up to 200 °C gives rise to a sharp interface and the well-known 45° rotation of the Fe lattice with respect to the MgO lattice. © *2011 American Institute of Physics*. [doi:10.1063/1.3554834]

I. INTRODUCTION

The epitaxial growth of oxides on semiconductors is a hot topic within the development of technological solutions aimed at adding new functionalities to conventional electronics or improving device performances. The case of high-k oxides on Si has been widely investigated in connection with the scaling down of complementary metal-oxide-semiconductor (CMOS) technology,[1] looking for suitable growth protocols to obtain sharp interfaces without oxidation, interdiffusion, and substrate amorphization. Currently there is renewed interest in Ge. As a result of its high electronic and hole mobilities, this material represents a promising candidate for the next generation of high performance complementary metal-oxide-semiconductor field-effect transistors (CMOSFETs). In this context, tunneling contacts through an insulating barrier hold potential for fixing the problem of high resistivity at the source and drain contacts for n-channel Ge MOSFET, due to the Fermi level pinning at the valence band maximum. Indeed, tunneling barriers (such as Al_2O_3 and MgO) between Ge and the metal contacts have been successfully used for this purpose.[2] In particular, MgO is particularly efficient for reducing the Schottky barrier and the concentration of interfacial defects, due to the good lattice matching between MgO and Ge, which allows for epitaxial growth.

Furthermore, MgO/Ge(001) epitaxial structures hold potential for the development of spintronics with Ge. In fact, the injection of a spin polarized current from a ferromagnetic electrode to a nonmagnetic semiconductor, or vice versa, requires the presence of an interfacial spin dependent resistance to overcome the problem of the resistance mismatch.[3] MgO tunneling barriers have been successfully employed to this scope, with performances remarkably better than those obtained by amorphous barriers (Al_2O_3).[4] GaAs was initially employed for applications exploiting spin optical pumping, and the epitaxial growth of MgO on GaAs has already been demonstrated.[5] Silicon has been also used, as a result of its primary role in electronics and long spin diffusion length, but its relevant chemical reactivity makes the realization of epitaxial structures quite difficult.[6] Germanium, instead, only very recently has deserved some attention.[7] Its high mobility, the opportunity of spin manipulation in Ge-based heterostructures,[8] and the possibility of spin optical pumping make Ge a good candidate for the development of semiconductor spintronics.

In this paper we present an experimental investigation of epitaxial growth of Fe/MgO/Ge(001) heterostructures, aiming to clarify how the different growth conditions influence the chemical and structural sharpness of the interfaces as well as the film crystallinity and the epitaxial relationship. In particular, the optimal growth conditions for achieving high-quality heterostructures suitable for the realization of tunneling contacts between Fe and Ge, with a transition region on the order of a single Ge unit cell at the MgO/Ge interface, in the case of n-doped Ge substrates consist of (a) room temperature (RT) growth of MgO followed by post annealing at 500 °C and (b) RT growth of Fe followed by annealing at 200 °C. This recipe gives rise to the Fe[100]//MgO[110]//Ge[100] epitaxial relationship reported also by other authors,[9,10] but interestingly enough we found that this is not uniquely determined by minimization of elastic energy in the MgO layer, as a mixture of grains presenting also the Fe[110]//MgO[100]//Ge[100] orientation is found in films grown with different recipes or on p-doped substrates.

[a)]Electronic mail: daniela.petti@mail.polimi.it.

 © 2011 American Institute of Physics

Author complimentary copy. Redistribution subject to AIP license or copyright, see http://jap.aip.org/jap/copyright.jsp

II. EXPERIMENTAL

The sample growth and *in situ* characterization were performed in an ultrahigh vacuum (UHV) system equipped with a molecular beam epitaxy (MBE) apparatus and a chamber for electron spectroscopies, as described in detail elsewhere.[11] Standard n-type Ge(001) ($n = 10^{15}$ cm^{-3} and $n = 10^{20}$ cm^{-3}) and p-type ($p = 10^{18}$cm^{-3}) wafers were used as substrates. After ultrasonic washing in isopropanol, the substrates were inserted into the UHV system and annealed at 650 °C for 1 h, with pressure below 2×10^{-9} mbar, in order to remove the native oxide. A further annealing at 730 °C for 20 min produced an ordered (2×1) reconstructed Ge(001) surface, as checked by reflection high-energy electron diffraction (RHEED) and low-energy electron diffraction (LEED). X-ray photoemission spectroscopy (XPS) revealed a negligible residual surface contamination (essentially O and C, below 3% in the probing depth of XPS). MgO was deposited at room temperature, at a rate of ~0.6 Å/min, by evaporation of pieces of stoichiometric MgO contained in a Ta crucible, heated by electron bombardment. The Fe overlayer, as well as the gold capping layer, was grown *in situ* by thermal evaporation of high purity metals. The thickness was estimated by using a quartz microbalance and then checked by XPS, especially for the MgO layer, the thickness of which is crucial for determining the tunneling resistance of the structure. Photoelectrons were excited with Al-Kα radiation ($h\nu = 1486.67$ eV) and analyzed by a 150 mm hemispherical analyzer (SPECS Phoibos 150). For the line shape analysis the pass energy was set to 10 eV, leading to a total resolution of 1 eV. The spectra have been collected both at 0° and at 60° emission angles with respect to the sample normal, the latter in order to increase the sensitivity to the interfacial oxidation state. *In situ* structural characterization of the MgO barrier was performed by X-ray photoelectron diffraction (XPD) polar scans of the O1s core level with Mg-Kα ($h\nu = 1253.67$ eV) and analyzer angular acceptance of ±1°. We chose O1s for two reasons: first, its high kinetic energy (720 eV, corresponding to an escape depth of 18.78 Å)[12] makes XPD sensitive to the whole thickness of MgO in the forward scattering regime; second, this peak is not superimposed on any Ge feature.

Scanning transmission electron microscopy and electron energy loss spectroscopy (STEM-EELS) experiments were carried out in a Nion UltraSTEM dedicated STEM operating at 100 kV and equipped with an Enfina spectrometer and a 5th-order aberration corrector. Principal component analysis (PCA) was used to remove random noise from the EEL spectra.[13] Specimens for STEM observations were prepared by conventional mechanical thinning and Ar ion milling.

III. RESULTS AND DISCUSSION

A. Optimization of the growth conditions

The first step in the fabrication of epitaxial Fe/MgO/Ge(001) heterostructures is the realization of a sharp interface between MgO and Ge. In order to find the optimum growth conditions we carried out a detailed investigation of the influence of substrate preparation, deposition temperature and post-annealing treatments on the interface quality.

For the substrate preparation, we investigated the effect of a controlled oxidation of the Ge(001) surface leading to the formation of exactly one monolayer of oxygen chemisorbed in the $p(1 \times 1)$O fashion. This way, Ge could be protected from further oxidation during MgO deposition in analogy with what happens for other surfaces such as Fe(001)-$p(1 \times 1)$O.[13,14] As described in detail elsewhere,[15] we found that this particular oxidized surface does not work efficiently as a passivating layer, while the clean $p(2 \times 1)$-Ge(001) surface represents the best substrate on top of which growth occurs with limited oxidation and amorphization of Ge.

For the MgO deposition on the clean $p(2 \times 1)$-Ge(001) surface we explored two different routes for achieving the best crystallinity of the MgO barrier compatible with interfacial sharpness: (1) RT growth of MgO followed by recrystallization via post-annealing and (2) growth of MgO at high temperature. For both routes we used XPS to monitor the level of oxidation of the Ge substrate and XPD for *in situ* quantitative analysis of the MgO crystallinity. The line shape of Ge $2p_{3/2}$ peak gives direct access to the degree of oxidation of Ge by virtue of the sizable chemical shift between the "metallic" component Ge^0 [binding energy (BE) = 1217.4 eV] and the other contributions coming from the different oxidation states Ge^{2+} (BE = 1219.2 eV) and Ge^{3+} (BE = 1220.2 eV).[16] The output of the optimization procedure of routes (1) and (2) can be summarized in two recipes which give the best results within each route: (R1) RT growth followed by annealing at 500 °C and (R2) growth at 300 °C without postannealing. Higher deposition temperatures and postannealing temperatures produced MgO barriers with lower crystallinity and higher oxidation of the Ge substrate.

In Fig. 1 we report the Ge $2p_{3/2}$ spectra taken at a 60° collection angle from 5 ML of MgO on Ge, grown according to recipes R1 and R2. It clearly appears that the shoulder at high binding energy, representative of Ge^{2+} and Ge^{3+} oxidation states (see the two minor peaks at 1219 and 1220 eV in the fitting of Fig. 1), is more evident in samples grown at 300 °C, thus indicating a higher substrate oxidation in the case of recipe R2. This can be ascribed to the different reactivity of Ge exposed to an oxygen flux (in this case O^- from MgO) at different temperatures; the formation of germanium oxide is indeed favored at 300 °C over room temperature conditions.[17] On the basis of this fact, it is reasonable that Ge oxidation is lower in the case of postgrowth annealing because in this condition the MgO crystal is fully formed and there will be competition between the dissociation of MgO and the formation of GeO_x. On the contrary, in the case of a high-temperature deposition, the presence of an O^- flux from MgO makes the Ge oxidation a process without an activation barrier, because it is not necessary to furnish further energy to the system, as the adatoms have already partially dissociated in Mg^+ and O^-.

In Table I we report the relative weight (Ge^{ox}/Ge^0) of oxidized interfacial Ge atoms (the sum of Ge^{2+} and Ge^{3+} components) with respect to the intensity of the main line from nonoxidized atoms. In all cases the Ge^{ox}/Ge^0 ratio is larger at the 60° collection angle, thus indicating an interfacial oxidation of Ge, while the lowest value (0.14 at 60° collection angle) is obtained on the sample grown at RT and then annealed at

Author complimentary copy. Redistribution subject to AIP license or copyright, see http://jap.aip.org/jap/copyright.jsp

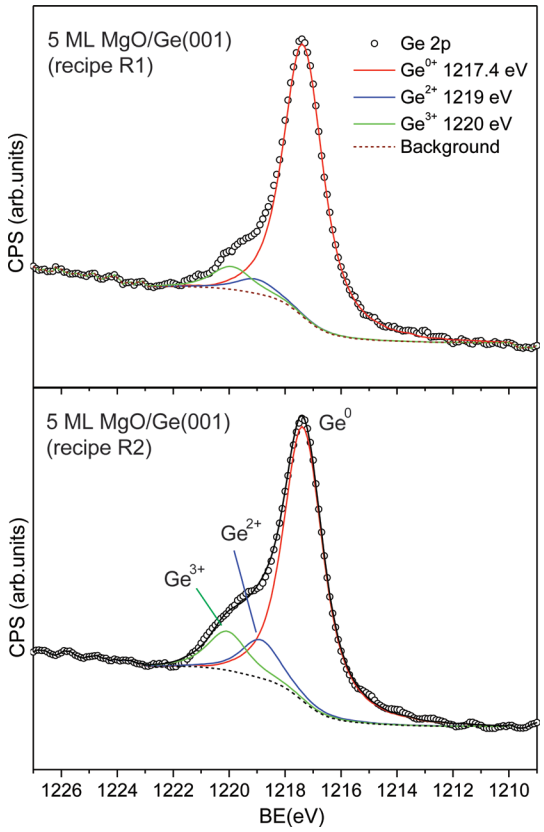

FIG. 1. (Color online) Comparison between the interfacial oxidation of Ge after MgO growth in two different conditions: R1: RT growth followed by annealing at 500 °C (top) and R2: growth at 300 °C without postannealing (bottom). Ge2p spectra taken at 60° collection angle are shown, indicating a much higher oxidation when recipe R1 is employed.

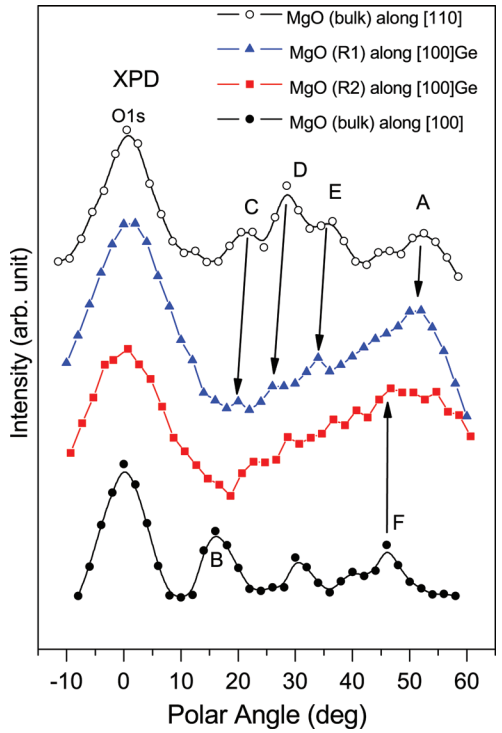

FIG. 2. (Color online) X-ray photoelectron diffraction (XPD) polar curves of O1s photoelectrons from a reference MgO single crystal (s.c.) with azimuth along the [100] (filled dots) and [110] (empty dots) directions, as well as XPD scans along the [100] of Ge, from MgO/Ge samples prepared with recipes R1 (triangles) and R2 (squares). The MgO thickness was 5 ML.

500 °C (R1). The deposition at 300 °C (R2) produces a higher Ge oxidation ($Ge^{ox}/Ge^0 = 0.28$ at 60° collection angle), which further increases up to 0.51 when a postannealing at 500 °C is performed. These results clearly indicate that recrystallization after RT growth gives the best results in terms of substrate oxidation, corresponding to a thickness of an interfacial GeO_x layer on the order of one monolayer.

At the same time, the investigation of the MgO structure via XPD indicates that recipe R1 gives better crystallinity with respect to R2. In Fig. 2 we report XPD polar curves from a reference MgO single crystal (s.c.) sample with azimuth along the [100] (filled dots) and [110] (empty dots) directions. XPD scans from MgO/Ge samples prepared with recipes R1 (triangles) and R2 (squares), both having a MgO thickness of 5 ML, are also shown, with azimuth along the [100] of Ge. First of all, note that the XPD curve from the sample prepared according to recipe R1 bears more similarity to the one from the MgO s.c. along the [110] azimuth, as indicated by the presence of peak A at 51° (present in the s.c. [110] scan) and the absence of peak B at 16° (evident in the s.c. [100] scan). Also, minor peaks (C,D,E) emerging from the background at about 19°, 25°, and 33° respectively, can be related to those at 21°, 27°, and 35° in the curve from the MgO s.c. along the [110] azimuth, with a shift toward low angles indicating that MgO grows compressed in plane. We conclude that MgO grows on Ge with the orientation MgO[110]//[Ge[100], at least in the case of samples prepared with recipe R1. On the other hand, the XPD scan on the MgO/Ge sample prepared with recipe R2 presents a line shape not well defined, bearing some similarities to the curve taken on MgO s.c. along the [100] direction (see for instance the absence of a well-defined peak A and the presence of feature F at 47° which is typical of a scan along the [100] direction of the MgO s.c.). From XPD data we can then conclude that, while recipe R1 gives rise to a well-defined crystalline structure,[18] R2 seems to produce a less ordered MgO film which could be a mixture of domains having the [100] direction parallel to the [100] and [110] direction of Ge.

TABLE I. Quantification of the relative weight of the components from oxidized interfacial Ge atoms, with respect to the main line from nonoxidized atoms, in $Ge2p_{3/2}$ XPS spectra taken at 0° and 60° collection angle.

Recipe	Ge^{ox}/Ge^0 at 0°	Ge^{ox}/Ge^0 at 60°
R1 (RT growth + annealing at 500 °C)	0.07	0.14
R2 (growth at 300 °C)	0.12	0.28
R2 + annealing at 500 °C	0.09	0.51

Concerning Fe growth, we found that RT growth[19] followed by annealing at 200 °C gives the best results in terms of crystallinity and sharpness of interfaces, while the standard procedure of postannealing up to 600 °C used for Fe/MgO/Fe tunneling junctions produces a sizable interdiffusion between MgO and the upper layer.[20] In the as-deposited sample, Fe is expected to be continuous[19] but no LEED pattern is present, indicating a limited long range ordering. This can be largely improved by annealing the sample, as

Author complimentary copy. Redistribution subject to AIP license or copyright, see http://jap.aip.org/jap/copyright.jsp

demonstrated by the appearance of a LEED pattern (data not shown) emerging from the background.

The high quality of MgO films epitaxially grown on Ge(001) following recipe R1 and of the entire Fe/MgO/Ge heterostructure can be appreciated in Fig. 3, where high resolution STEM images are reported from a slice with surfaces parallel to (−110) planes of Ge. The MgO film is continuous over large distances [Fig. 3(a)] and a high level of epitaxy is observed both on the MgO and Fe layers [Fig. 3(b)]. Furthermore, the transition zone at the MgO/Ge interface has a thickness on the order of one Ge unit cell (5.66 Å), as confirmed by chemical profiles taken with EELS [Fig. 3(c)] along a line perpendicular to the interface. The Ge and Mg signals change from 75% to 25% of their maximum value within a single unit cell. This finding represents a significant improvement with respect to the best data reported in literature for MgO films grown at 250 °C on Ge,[9] where the transition region extends over more than two Ge unit cells. The higher sharpness observed by STEM in our samples grown at RT and then annealed at 500 °C (according to recipe R1), with respect to the samples reported in literature (grown directly at high temperature), is fully coherent with our XPS study on the oxidation presented above.

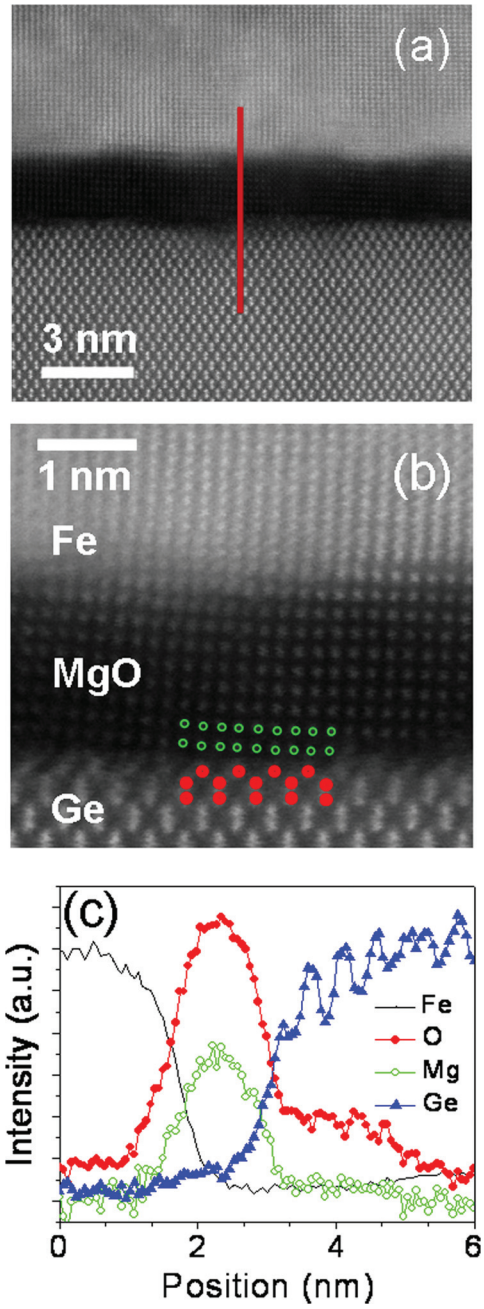

FIG. 3. (Color online) High-resolution STEM images of the full Fe/MgO/Ge heterostructure grown on n-doped Ge. (a) Cross section of a large area; the line marks where the EELS linescan was acquired. (b) Zoom across the MgO barrier; the Ge and the Mg-O columns are highlighted in red (filled dots) and in green (empty dots), respectively. (c) Elemental profile along the interface, as measured by EELS, indicating that interdiffusion is, at most, limited to a single Ge unit cell.

B. Epitaxial relationships

From inspection of the high-resolution STEM image shown in Fig. 3(b), the epitaxial relationship in the Fe/MgO/Ge structure clearly appears. Because the slice was cut with planes perpendicular to the (−110) planes of Ge, the typical hexagonal structure appears, where each vertex is occupied by a couple of columns corresponding to the two atoms of the basis of the Ge lattice, which can be considered as a fcc with a basis. On top of Ge the cubic structure of MgO is visible, with the spacing between Mg-O columns corresponding to half of the diagonal of the cubic unit cell of Ge. This fact indicates that the [100] direction of MgO is parallel to the [110] direction of Ge, i.e., that in these conditions MgO grows on Ge with a rotation of 45°. The Fe overlayer displays a square lattice which is coherent with a rotation of 45° with respect to that of the MgO layer, as is usual for epitaxial growth of Fe on MgO,[21] thus indicating that the [100] direction of Fe is parallel to the [100] direction of Ge. Note that misfit dislocations are localized at the MgO/Ge and Fe/MgO interfaces. Some buckling of the MgO layers away from the interface plane is observed, most likely to accommodate steps on the Ge surface.

Further confirmation of the epitaxial relationship derived from STEM images comes from the RHEED data reported in Fig. 4. Figures 4(a) and 4(b) show the diffraction patterns from the clean Ge(001) surface, with the incident beam along [100] and [110] respectively. In the latter, we note the presence of the half order streaks, indicating a (2×1) reconstruction of the surface. Figures 4(c) and 4(d) 4(e) and 4(f) correspond to the MgO (Fe) layer measured along the azimuths [100] and [110] of the substrate, respectively. In Figs. 4(g) and 4(h) the primitive cells of the direct surface two-dimensional lattices of Ge(001), MgO(001), and Fe(001) are sketched. The direct lattices are oriented as indicated by HRTEM, that is Fe[100]//MgO[110]//Ge//[100] With the incident beam along the [100] of Ge, the spacings between adjacent streaks (or points) in RHEED patterns are $4\pi/a_{Ge}$, $2\sqrt{2}\pi/a_{MgO}$, and $2\pi/a_{Fe}$ in Ge, MgO, and Fe respectively (thick arrows in Fig. 4, blue online). Assuming a relaxed surface, and employing bulk lattice parameters ($a_{Fe} = 2.87$ Å, $a_{MgO} = 4.21$ Å and $a_{Ge} = 5.66$ Å), we get values for the ratios $(2\sqrt{2}\pi/a_{MgO})/(4\pi/a_{Ge})$ and $(2\sqrt{2}\pi/a_{MgO})/(2\pi/a_{Fe})$ equal to 0.95 and 0.96, to be

Author complimentary copy. Redistribution subject to AIP license or copyright, see http://jap.aip.org/jap/copyright.jsp

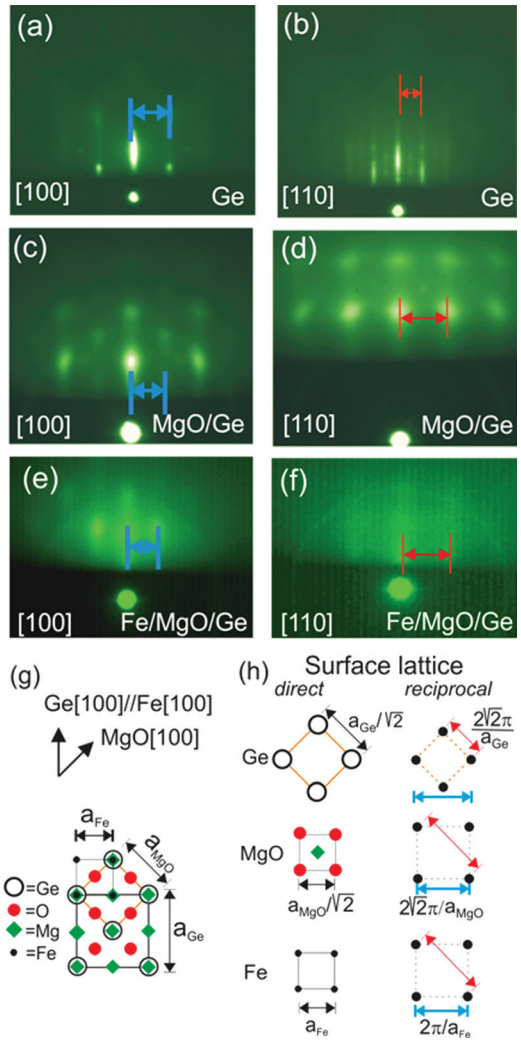

FIG. 4. (Color online) RHEED patterns of Ge (a), (b), MgO (c), (d) and Fe (e), (f) layers taken along the [100] (left columns) and [110] (right column) directions of Ge substrate. The epitaxial relationship between Ge, MgO, and Fe is shown in (g), while the direct and reciprocal lattices are sketched in (h).

compared with the experimental values 0.94 ± 0.04 and 0.97 ± 0.04. Analogously, we get $(4\pi/a_{MgO})/(2\sqrt{2}\pi/a_{Ge}) = 1.90$ and $(4\pi/a_{MgO})/(2\sqrt{2}\pi/a_{Fe}) = 0.96$ along the [110] direction of the Ge substrate (thin arrows in Fig. 4, red online) to be compared with the experimental values 1.90 ± 0.08 and 0.97 ± 0.1. The very good agreement between RHEED data and calculations confirms that MgO definitely grows on Ge with an in-plane lattice rotation of 45°, and that the Fe lattice is aligned, cube on cube, to the Ge lattice.

While the Fe-MgO epitaxial relationship is well known, for the MgO/Ge interface the situation is much less well understood. In fact, two epitaxial relationships are predicted within the lattice matching epitaxy (LME) and domain matching epitaxy (DME) approaches,[22] MgO[100]//Ge[110] and MgO[100]//Ge[100] respectively. According to LME, growth takes place by one-to-one matching of the lattice constants for lattice mismatch less than the critical value of 7–8%, so that MgO prefers to rotate its lattice by 45° in order to get a lattice mismatch with Ge of 5.2%, compared to the 25.6% misfit for the cube-on-cube growth. On the other hand, DME theory predicts that, for systems with relatively large lattice mismatch on the single unit cell, epitaxy can occur by matching integral multiples of lattice cells. For MgO growth on Ge the MgO[100]//Ge[100] relationship would indeed produce a misfit of −0.7% if a 4:3 lattice ratio is assumed. The latter situation has been experimentally found in the case of MgO in Si(001) and GaAs(001), corresponding to lattice misfits of 3.4% and −0.7%.[5,6] The fact that two systems like MgO/Ge and MgO/GaAs, absolutely identical from the point of view of lattice mismatch, present a completely different epitaxial relationship clearly indicates that a major role is played by interfacial energy connected to chemical interactions. The more evident difference between GaAs(001) and Ge(001) surfaces is that the first is polar, while the second is neutral; thus a major impact of the surface electrostatics on the epitaxial relationship is expected as well. To check this point we performed a STEM analysis on MgO/Ge(001) interfaces grown following the same recipe (R1) onto substrates doped differently: n+ (10^{20} cm^{-3}) and p (10^{18} cm^{-3}). Interestingly, data on samples grown onto n+ substrates show the same epitaxial relationship depicted above, i.e., MgO[100]//Ge[110] along all the cross sections examined, while in case of samples grown onto p-doped Ge the coexistence of domains with MgO[110]//Ge[100] and MgO[100]//Ge[100] alignment is found. High angle ADF images reveal the occasional presence of Fe grains with a different orientation, [110], as shown in Fig. 5. The corresponding fast Fourier transform (FFT) clearly shows different zone axes of the Fe grains, [110] on the left and [100] on the right. Notice the change in orientation of the MgO grains as well, undergoing a 45° rotation along the *z*-axis which ultimately modifies the Fe layer. Only a few of these misoriented grains have been found, though, and their size remains small (~10 nm). These changes might be due to the nucleation of MgO grains with a different orientation. Note that the moderate p-doping (10^{18} cm^{-3}) and the use of Ga as dopant, which has a ionic radius very similar to that of Ge, allows us

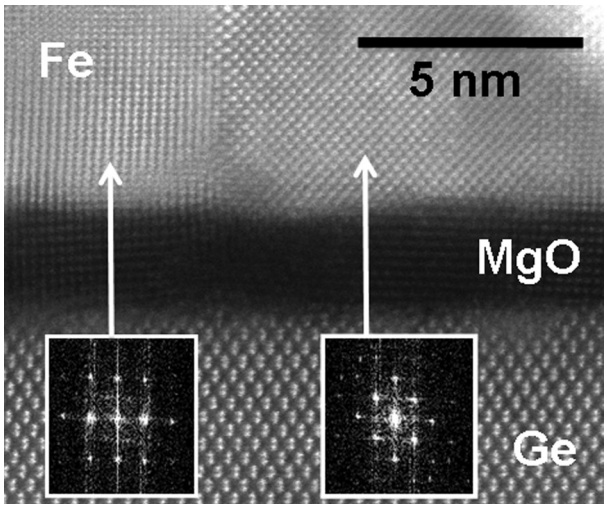

FIG. 5. High-resolution STEM images of the full Fe/MgO/Ge heterostructure grown on p-doped Ge showing, the boundary between two grains displaying different orientations of the Fe and MgO overlayers. The insets show the FFT of the corresponding Fe grains (Refs. 1–10), and [100] zone axis, respectively, marked with arrows.

Author complimentary copy. Redistribution subject to AIP license or copyright, see http://jap.aip.org/jap/copyright.jsp

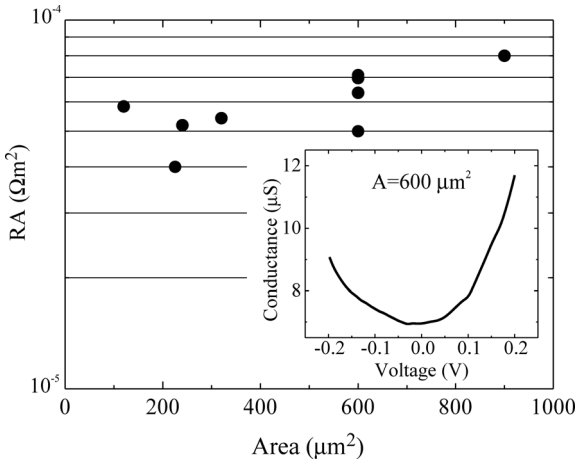

FIG. 6. Resistance per area (RA) plot as a function of the junction area. In the inset the typical parabolic shape of the conductance of a tunneling junction 600 μm^2 in area is shown.

to exclude surface strain effects like those found in boron-doped silicon-germanium alloys.[23]

These facts, in conjunction with the not perfectly defined crystallographic orientation seen from XPD on samples grown with recipe R2, clearly indicates that in case of MgO growth on Ge the epitaxial relationship is not strongly and uniquely driven by minimization of elastic energy, so that other aspects such as growth conditions and also substrate doping can influence the crystallographic orientation of the MgO film. A deeper understanding of these phenomena is definitely beyond the scope of this work and would require *ab initio* calculations of the interface free energy for the different epitaxial relationships.

C. Tunneling junctions

The continuity of the MgO barrier over long distances observed by TEM is a good starting point for fabricating tunnel devices and checking if the transport is dominated by tunneling. To this aim, tunneling junctions have been fabricated via optical lithography, with areas ranging from 30 to 900 μm^2, in which the bottom and top electrodes coincide with the Ge substrate and Fe overlayer, respectively. The conductance curves, like the one reported in the inset of Fig. 6 and measured at RT, present the typical parabolic shape of tunneling junctions, clearly indicating that tunneling is the dominant mechanism. The relevant parameter, i.e., the resistance per area product (RA), has been evaluated on junctions with different size but with the same MgO thickness (2.5 nm) at a bias voltage of 0.2 V, as reported in Fig. 6. For devices fabricated on a slightly n-doped substrate (10^{15} cm^{-3}) we found an almost constant RA product, on the order of 5×10^{-5} Ωm^2, on the size of and similar to the values reported in literature for the same system.[24]

IV. CONCLUSIONS

In summary, in this paper we demonstrate the epitaxial growth of high quality Fe/MgO/Ge(001) heterostructures suitable for the realization of tunnel contacts between a ferromagnet and Ge. We find that the best way to achieve good crystallinity of the MgO barrier and sharp interfaces is by growing MgO at RT on a Ge-p(2×1) surface and then performing a postannealing at 500 °C. Analogously, the Fe overlayer is grown at RT and then annealed up to 200 °C, as higher annealing temperatures produce strong interdiffusion. The epitaxial relationship between the different layers is Fe[100]//MgO[110]//Ge[100] with a 45° rotation of the MgO lattice with respect to Ge for RT growth and subsequent recrystallization at 500 °C on n-doped Ge. Interestingly, a mixture of Fe[100]//MgO[110]//Ge[100] and Fe[110]//MgO[100]//Ge[100] grains is observed for different growth conditions or p-doped substrates. These results indicate that in the case of MgO/Ge(001) the epitaxy is not simply driven by the minimization of the elastic energy in the MgO barrier, but that interfacial free energy plays a major role. The high quality of the heterostructures synthesized is confirmed by transport measurements on tunneling junctions, displaying the typical parabolic conductance and RA values on the order of 5×10^{-5} Ωm^2 for an MgO barrier 2.5 nm thick on slightly n-doped Ge.

ACKNOWLEDGMENTS

The authors would like to thank M. Leone for his skillful technical assistance and F. Ciccacci, G. Isella, and S. Bietti for valuable discussions. This work was funded by Fondazione Cariplo via the project MANDIS (Project No. 2007.5095). Research at ORNL (MV) was supported by the Office of Science, Materials Sciences and Engineering Division of the US Department of Energy. J. Gazquez acknowledges financial support from the European Research Council Starting Investigator Award (Grant No. 239739 STEMOX). The authors are thankful to J.T. Luck for STEM specimen preparation and to M. Watanabe for the PCA plug-in for Digital Micrograph.

[1]R. A. McKee, F. J. Walker, and M. F. Chisholm, Phys. Rev. Lett. **81**, 3014 (1998).
[2]Y. Zhou, M. Ogawa, X. Han and K. L. Wang, Appl. Phys. Lett. **93**, 202105 (2008); Y. Zhou, M. Ogawa, M. Bao, W. Han, R. K. Kawakami and K. L. Wang, Appl. Phys. Lett. **94**, 242104 (2009); Y. Zhou, W. Han, Y. Wang, F. Xiu, J. Zou, R. K. Kawakami, and K. L. Wang, Appl. Phys. Lett. **96**, 102103 (2010).
[3]A. Fert and H. Jaffrès. Phys. Rev. B **64**, 184420 (2001); P. C. van Son, H. van Kempen, and P. Wyder, Phys. Rev. Lett. **58**, 2271 (1987).
[4]X. Jiang, R. Wang, R. M. Shelby, R. M. MacFarlane, S. R. Bank, J. S. Harris, and S. S. P. Parkin, Phys. Rev. Lett. **94**, 056601 (2005).
[5]L. S. Hung, L. R. Zheng, and T. N. Blanton, Appl. Phys. Lett. **60**, 3129 (1992).
[6]G. X. Miao, J. Y. Chang, M. J. van Veenhuizen, K. Thiel, M. Seibt, G. Eilers, M. Münzenberg, and J. S. Moodera, Appl. Phys. Lett. **93**, 142511 (2008).
[7]E. J. Loren, B. A. Ruzicka, L. K. Werake, H. Zhao, H. M. van Driel, and A. L. Smirl, Appl. Phys. Lett. **95**, 092107 (2009).
[8]S. D. Ganichev, S. N. Danilov, V. V. Bel'kov, S. Giglberger, S. A. Tarasenko, E. L. Ivchenko, D. Weiss, W. Jantsch, F. Schäffler, D. Gruber, and W. Prettl, Phys. Rev. B **75**, 155317 (2007).
[9]W. Han, Y. Zhou, K. L. Wang, and R. K. Kawakami, J. Cryst. Growth **312**, 44 (2009).
[10]Kun-Rok Jeon, Chang-Yup Park, and Sung-Chul Shin, Crystal Growth and Design, **10**, 1346 (2010).
[11]R. Bertacco, M. Cantoni, M. Riva, A. Tagliaferri, and F. Ciccacci, Appl. Surf. Sci. **252**, 1754 (2005).
[12]S. Tanuma, C. J. Powell, and D. R. Penn, Surf. Interface Anal **17**, 927 (1991).

Author complimentary copy. Redistribution subject to AIP license or copyright, see http://jap.aip.org/jap/copyright.jsp

[13]M. Bosman, M. Watanabe, D. T. L. Alexander, and V. J. Keast; Ultramicroscopy **106**, 1024 (2006).
[14]R. Bertacco, M. Merano, and F. Ciccacci; Appl. Phys. Lett. **72**, 2050 (1998).
[15]M. Cantoni, D. Petti, C. Rinaldi, and R. Bertacco, Microelectron. Eng. **88**, 530.
[16]K. Prabhakaran and T. Ogino, Surf. Sci. **326**, 263 (1995).
[17]A. Molle, Md. N. K. Bhuiyan, G. Tallarida, and M. Fanciulli, Appl. Phys. Lett. **89**, 083504 (2006).
[18]Also in the as deposited sample, XPD data (not shown) reveal the presence of a noticeable degree of crystallinity, which is improved through the postgrowth annealing. Indeed, in the XPD curve the characteristic peaks at 0° and 51° collection angles are quite evident, while minor features (such as the peaks C, D, E in Fig. 2) barely emerge from the background.
[19]A. Bona, C. Giovanardi, S. Valeri, Surf. Sci. **498**, 193 (2002).
[20]D. Petti, M. Cantoni, C. Rinaldi, and R. Bertacco, "Chemical and electronic properties of Fe/MgO/Ge heterostructures for spin," J. Phys.: Conf. Ser. (to be published).
[21]S. Yuasa, T. Nagahama, A. Fukushima, Y. Suzuki, and K. Ando, Nature Mater. **3**, 868 (2004).
[22]J. Narayan and B. C. Larson, J. Appl. Phys. **93**, 278 (2003).
[23]S. Chopra, M. C. Ozturk, V. Misra, K. McGuire, and L. E. McNeil, Appl. Phys. Lett. **88**, 202114 (2006).
[24]K.-R. Jeon, B.-C. Min, H.-S. Lee, I.-J. Shin, C.-Y. Park, and S.-C. Shin, Appl. Phys. Lett. **97**, 022105 (2010).

Author complimentary copy. Redistribution subject to AIP license or copyright, see http://jap.aip.org/jap/copyright.jsp